Electronic Research Archive

http://www.aimspress.com/journal/era

ERA, 30(10): 3660–3678.
DOI: 10.3934/era.2022187
Received: 10 May 2022
Revised: 22 July 2022
Accepted: 29 July 2022
Published: 03 August 2022

Research article

Identify the characteristic in the evolution of the causality between the gold and dollar

Ping Wang, Changgui Gu*, Huijiu Yang and Haiying Wang

Business School, University of Shanghai for Science and Technology, Shanghai 200093, China

* **Correspondence:** Email: guchanggui@usst.edu.cn.

Abstract: The causal inference method based on the time-series analysis has been subject to intense scrutiny, by which the interaction has been revealed between gold and the dollar. The positive or negative causality between them has been captured by the existing methods. However, the dynamic interactions are time-varying rather than immutable, i.e., the evolution of the causality between gold and the dollar is likely to be covered by the statistical process. In this article, a method which combines the pattern causality and the state-transition network is developed to identify the characteristics of the causality evolution between gold and the dollar. Based on this method, we can identify not only the causality intensity but also the causality type, including the types of positive causality, negative causality and the third causality (dark causality). Furthermore, the patterns of the causalities for the segments of the bivariate time series are transformed to a state-transition network from which the characteristics in the evolution of the causality have also been identified. The results show that the causality has some prominent motifs over time, that are the states of negative causality. More interestingly, the states that act as a bridge in the transition between states are also negative causality. Therefore, our findings provide a new perspective to explain the relatively stable negative causality between gold and the dollar from the evolution of causality. It can also help market participants understand and monitor the dynamic process of causality between gold and the dollar.

Keywords: causal inference; time-series analysis; pattern causality; state-transition network; motif

1. Introduction

The dollar is an international currency issued and endorsed by the Federal Reserve. As a stable currency, it is used for the most extensive payment and settlement. Gold is a precious metal, which contains commodity and monetary attributes. Accordingly, both have integrated vital risk aversion functions, whose has always been a concern to the financial media and the investors. So far, there have been multiple studies on the relationship between the gold price and the dollar index [1–7]. Most

studies showed a significant negative correlation between them [8–10]; when the dollar depreciates, the nominal price of gold will rise. Therefore, gold behaves as a hedge against the dollar and provides exchange rate hedging for investors holding the dollar. On the contrary, observers have long noted a positive correlation of them, although this correlation will not last long [3, 11–14]. Moreover, the relationship is not always stable [1, 15]. When the financial markets run smoothly, gold and the dollar will show a trend of going up and falling on the other; and when there is a local political crisis or economic crisis in the world, the correlation will be positive.

The previous studies have obtained time-varying causal relationships between gold and the dollar based on the econometric framework [1, 15], such as the error correction model, the standard bivariate $GARCH$ models and the extension to the structural $BEKK$ model. In addition, Lin et al. [16] utilized wavelet analysis to decompose the pair relations between oil-US dollar and gold-US dollar into short-term and long-term parts, they found that the pair relationship becomes weaker in the long run and the short-run correlations are much higher after the early $1990s$. Moreover, Mo et al. [3] investigated the long-term relationship by means of both fractional cointegration and $DCC-MGARCH$ method and employed non-linear asymmetric causality to examine the effect of the 2007 global financial crisis on the short-term interdependence. However, both the causality's evolution rule and motif structure were ignored in these studies. It is still an open issue to discover the motifs and their relationships. The combined application of time-series analysis and complex network theory effectively describes the temporal evolution of relationships in complex systems [17–19]. Methods of complex networks have been proposed to analyze time series, such as visibility graph methods [20], recurrence network method [21], coarse-graining method [22], pseudo-periodic time series [23], quasi-isometric transformation [24], correlation matrix [25] and the state-transition network [26–28]. These methods can map the time series into the network. In this article, we apply the state-transition network method of easy-to-operate to convert the time series into a complex network. The method can reveal dynamic information as well as complicated behaviour in complex systems.

In recent years, causal analysis has attracted the attention of many researchers because it can reveal the internal laws between variables. For example, the Granger causality test has successfully revealed the non-linear causal relationship of separable variables [29, 30]; transfer entropy can detect causality based on the information flowing between variables, by which the large sample size is required to estimate accurately [31]. Moreover, the cross-convergent mapping (CCM) indicates that the time-series variables are causally linked if they are from the same dynamical system. Namely, they share a common attractor [32, 33]. It can distinguish the causality from the correlation in inseparable systems, which complements the Granger causality test. The weakness for the CCM method is that it is sensitive to noise of which the influence inevitably exists in natural systems.

In order to decrease the impact of noise, Stavroglou et al. proposed the pattern causality algorithm (PC) to investigate the symbolic dynamics based on the CCM [34, 35]. The PC method can judge not only the causality intensity but also the causality type, by which the causality is divided into three types, i.e., positive, negative, and dark (a more complex causal relationship). The targeted partition allows the unique identification for both persistent causal structures and dominant influences that would otherwise be lost in the noise of disparate causalities(if we did not discern the three types of interactions). Moreover, this method reveals causality between variables from the perspective of non-linear dynamics.

In this article, a state-transition network was built to detect the evolutional or time-varying characteristics in the causality between gold price and the dollar index. Specifically, the idea is to extract all possible segments from the initial bivariate time-series of gold price and the dollar index by a sliding window. Then, for each segment, the non-linear causality is identified by the *PC* method, containing the causality type as well as causality intensity. The causality pattern is used to describe the state. We mapped all the states defined as nodes to a unique state chain. An edge is added between two states(nodes) if they appear successively. The resulting network is called a state-transition network whose topological structure can represent the dynamic characteristics of the causal relationship. Thus, the results of this paper provide a reference for studying the time-varying characteristics of causality between gold and the dollar. The structure of this article is as follows. In Section II, we present (i) the data description of gold and the dollar analyzed in this study; (ii) the steps of the method that combines *PC* and state-transition network; (iii) definitions of concepts; Section III shows (i) determination of an appropriate window size; (ii) identification of important causality states; (iii) identification of the transitions among nodes and among clusters, respectively; Section IV summarizes and discusses the results.

2. Materials and methods

2.1. Data description and data preprocessing

The daily closing prices of gold futures and the dollar index futures, respectively, were downloaded from the website, https://cn.investing.com/. They are issued by the Intercontinental Exchange of the United States, of which stock exchange codes are *ZG* and *DX*, respectively. The data was selected from November 21, 1985 to June 22, 2022. The length of the bivariate series is 9248 after deleting a small number of missing data (63 data points of gold and 83 data points of the dollar). Note that Saturdays and Sundays are excluded from the time series. Because the original data is unstable and there is a large difference between gold and the dollar, we performed the analysis based on the logarithmic return rate of daily closing prices.

2.2. Methods

The specific process for building the state-transition network consists of the following five steps: (i) dividing the time series into segments of the equal length; (ii) obtaining the reconstructed phase space for each fragment; (iii) calculating the causality types as well as the causality intensities by the *PC* method; (iv) transforming the causality types and the causality intensities into causality states; (v) constructing the state-transition network. The whole process is shown in Figure 1.

Step 1. Dividing the time series into segments of equal length.

For simplicity, let X and Y represent gold and the dollar, respectively. X and Y can be expressed as time series $X = X(1), \cdots, X(N)$ and $Y = Y(1), \cdots, Y(N)$, respectively, where N is the length of time series. Let the window size be w and the sliding step be 1. Accordingly, $N - w + 1$ fragments are obtained for each time series. Then, the i_{th} fragment can be expressed as:

$$\begin{aligned} X^i &= \{X(i), X(i+1), \cdots, X(i+w-1)\}, 1 \le i \le N-w+1, \\ Y^i &= \{Y(i), Y(i+1), \cdots, Y(i+w-1)\}, 1 \le i \le N-w+1. \end{aligned} \tag{2.1}$$

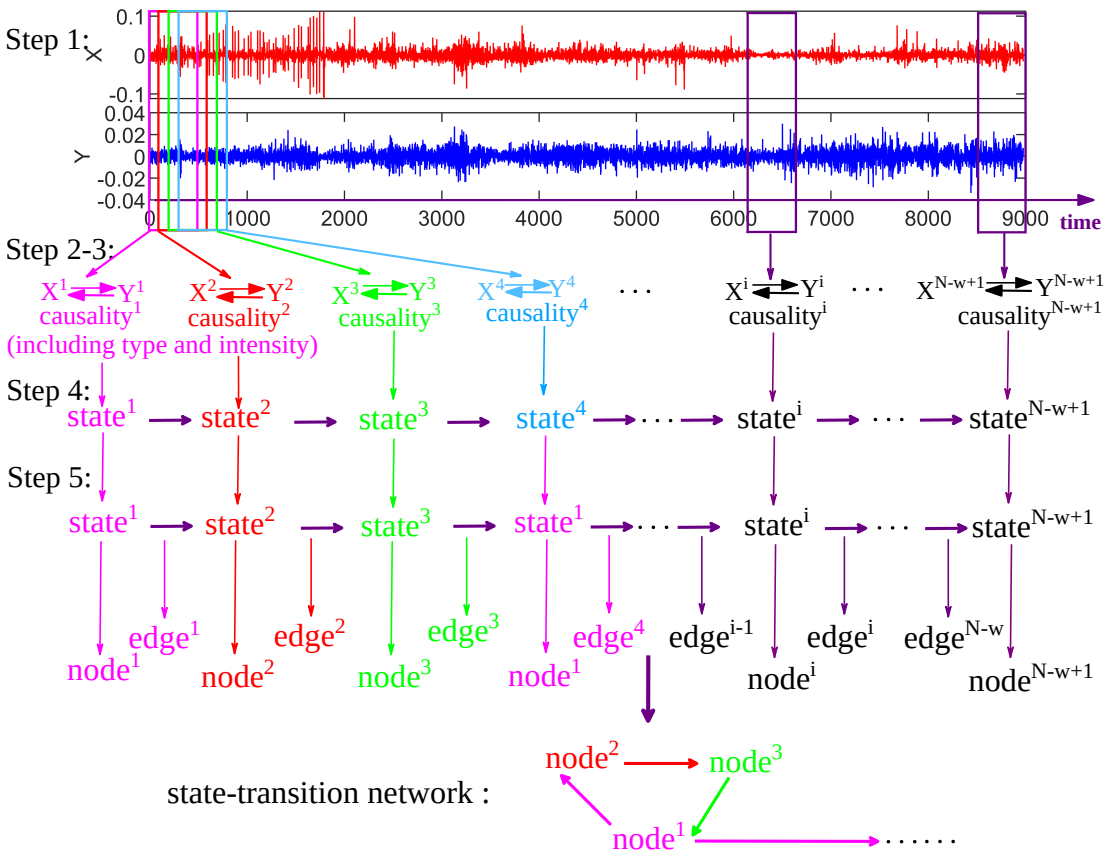

Figure 1. (color online) The process of constructing the causality network between two variables X and Y.

Step 2. Obtaining the reconstructed phase space for each fragment.

We reconstructed the phase space for each fragment defined by Eq (2.1) [36, 37]. E and τ represent the embedded dimension and delay time, respectively. A data point is an E-dimensional vector in the phase space [37]. The j_{th} point in the pase space of the i_{th} fragment can be expressed as

$$x(j) = \left\{X^i(j), X^i(j+\tau), X^i(j+2\tau), \cdots, X^i(j+(E-1)\tau)\right\}, 1 \le i \le N-w+1, 1 \le j \le w-(E-1)\tau, \tag{2.2}$$

where E and τ are the two parameters of which values are required to be determined. Their values will affect the accuracy of the results. If the values are too large, the system will lose much important information; and if the values are too small, the system will be easily disturbed by noise. A great deal of work have been done around this issue. In this article, the $C-C$ method [38] is utilized to determine the values of E and τ, simultaneously. By this method, the optimal embedding dimensions were obtained for the two variables X, Y are 2 and 3, respectively. The values of the dimensions are also limited by the application of PC method, i.e., the embedding dimension of each variable should be the same and the missing information of the system should be as little as possible. Therefore, the values of E and τ were set to 3 and 1 in this article, respectively. According to Eq (2.2), i_{th} fragment of

X can be expressed in the phase space by the matrix MX^i:

$$\begin{aligned} X^i &= \{X(i), X(i+1), \cdots, X(i+w-1)\} \Rightarrow MX^i \\ &= \begin{pmatrix} x(1) & = \left\{X^i(1), X^i(1+\tau), \cdots, X^i(1+(E-1)\tau)\right\} \\ x(2) & = \left\{X^i(2), X^i(2+\tau), \cdots, X^i(2+(E-1)\tau)\right\} \\ \vdots & \\ x(w-(E-1)\tau) & = \left\{X^i(w-(E-1)\tau), X^i(w-(E-2)\tau), \cdots, X^i(w)\right\} \end{pmatrix}, \end{aligned} \tag{2.3}$$

Similarly, we can obtain the matrix MY^i by Eq (2.3).

Step 3. Calculating the causality patterns as well as the causality intensities.

PC is a method proposed by Stavroglou et al. to explore nonlinear causality between time series developed from *CCM* [34]. It can judge not only the the causality intensity but also the causality type. The *PC* method is described as below. The distance matrix $DX^i$is defined as:

$$DX^i = \begin{pmatrix} d(x(1),x(1)) & d(x(1),x(2)) & \cdots & d(x(1),x(w-(E-1)\tau)) \\ d(x(2),x(1)) & d(x(2),x(2)) & \cdots & d(x(2),x(w-(E-1)\tau)) \\ \vdots & \vdots & \vdots & \vdots \\ d(x(w-(E-1)\tau),x(1)) & d(x(w-(E-1)\tau),x(2)) & \cdots & d(x(w-(E-1)\tau),x(w-(E-1)\tau)) \end{pmatrix}, \tag{2.4}$$

where $d(x(t), x(t+1))$ is the Euclidean distance from $x(t)$ to $x(t+1)$ for a focused time t. According to Eq (2.4), $E+1$ real nearest neighbors for $x(t)$ represented by $NN_{x(t)}$ were found in Eq (2.5). The reason why we chose $E+1$ nearest neighbor was that it requires at least $E+1$ point to form bounded simplicity in E-dimensional phase space. From these $E+1$ nearest neighbors, two pieces of information were recorded, i.e., their time indexes $t_{x_1}, t_{x_2}, \cdots, t_{x_{E+1}}$, and their distance from a focused point $x(t)$. Similarly, we can obtain $y(t)$'s $E+1$ nearest neighbors and their time indices $t_{y_1}, t_{y_2}, \cdots, t_{y_{E+1}}$. These time indices corresponding to the nearest neighbors to $y(t)$ on MY^i are used to identify the points in MX^i, i.e., $x(t)$'s $E+1$ estimated nearest neighbors by $y(t)$. Thus, the distances from $x(t)$ to $x(t)$'s $E+1$ real nearest neighbors and the distances from $x(t)$ to $x(t)$'s $E+1$ estimated nearest neighbors by $y(t)$ are shown in Eq (2.6).

$$\begin{aligned} NN_{x(t)} &= min_{(E+1)}\{d(x(t),x(1)), d(x(t),x(2)), \cdots, d(x(t),x(t-(E-1)\tau))\} \\ &= \{NN_{x(t_1)}, NN_{x(t_2)}, \cdots, NN_{x(t_{E+1})}\} \\ &\Rightarrow < t_{x_1}, t_{x_2}, \cdots, t_{x_{E+1}} >, \end{aligned} \tag{2.5}$$

$$\begin{aligned} d_j &= d(x(t), x(t_{x_j})), 1 \le j \le E+1 \\ \hat{d}_j &= d(x(t), x(t_{y_j})), 1 \le j \le E+1 \end{aligned} \tag{2.6}$$

The real pattern of the MX^i's t_{th} point $x(t)$ is:

$$Pattern_{x(t)} = signature(sig_{x(t)}), \tag{2.7}$$

where

$$sig_{x(t)} = \sum_{j=1}^{E+1} W_j s_j,$$

$$W_j = \frac{e^{d_j}}{\sum_{j=1}^{E+1} e^{d_j}}, 1 \le j \le E+1,$$

$$s_j = \left(\frac{X(t_j - \tau) - X(t_j)}{X(t_j)}, \frac{X(t_j - 2\tau) - X(t_j - \tau)}{X(t_j - \tau)}, \cdots, \frac{X(t_j - (E-1)\tau) - X(t_j - (E-2)\tau)}{X(t_j - (E-2)\tau)} \right), 1 \le j \le E+1,$$

where the function *signature* stands for symbolization. In particular, when $sig_{y(t)}$ is greater than 0, $Pattern_{y(t)}$ stands for $\nearrow$; when $sig_{y(t)}$ is less than 0, $Pattern_{y(t)}$ stands for $\searrow$; when $sig_{y(t)}$ is equal to 0, $Pattern_{y(t)}$ stands for $\rightarrow$. Furthermore, the estimated pattern of the MX^i's t_{th} point $x(t)$ by MY^i's t_{th} point $y(t)$ is:

$$\hat{Pattern}_{x(t)} = signature(\hat{sig}_{x(t)}), \tag{2.8}$$

where

$$\hat{sig}_{x(t)} = \sum_{j=1}^{E+1} \hat{W}_j s_j,$$

$$\hat{W}_j = \frac{e^{\hat{d}_j}}{\sum_{j=1}^{E+1} e^{\hat{d}_j}}, 1 \le j \le E+1.$$

Similarly, the real pattern and the estimated pattern of each point in MX^i and MY^i can also be obtained, $i = 1, 2, ..., N - w + 1$. All the situations of PC pattern are shown for $E = 3$ in Figure 2. The left blue striped, right red striped, and purple boxes represent positive causalities, negative causalities and dark causalities, respectively. We recorded the point with the same pattern of $Pattern_{x(t)}$ and $\hat{Pattern}_{x(t)}$, i.e., the accurately estimated point. Each cell (the box in Figure 2) is filled with proportion of each pattern in the total accurately predicted points. Thus, the value of each cell is in the range from 0 to 1. The causality type of X on Y is the largest number's pattern in the i_{th} fragment denoted as $p^i_{X\to Y}$; and the causality intensity is the proportion of the largest number's pattern in all patterns denoted as $s^i_{X\to Y}$. By repeating this process, we can obtain both the causality type and the causality intensity from X to Y and from Y to X for all fragments.

Step 4. Transforming causality types and causality intensities into causality states.

The causality type and the causality intensity are transformed into a particular state, i.e., coarse-grained local features while retaining only some large-scale features. A four-letter string represents the state of each fragment. The first and third letters represent the causality type from X to Y and from Y to X, respectively, and the second and fourth letters represent the causality intensity from X to Y and from Y to X. For example, the first and second letters can be obtained by the following formula,

$$Type^i_{X\to Y} = \begin{cases} P, & p^i_{X\to Y} = Positive \\ N, & p^i_{X\to Y} = Negative, \\ D, & p^i_{X\to Y} = Dark \end{cases} \quad 1 \le i \le N - w + 1, \tag{2.9}$$

$$Intensity^i_{X\to Y} = \begin{cases} a, & 0.8<s^i_{X\to Y} \le 1 \\ b, & 0.6<s^i_{X\to Y} \le 0.8 \\ c, & 0.4<s^i_{X\to Y} \le 0.6, \\ d, & 0.2<s^i_{X\to Y} \le 0.4 \\ e, & 0 \le s^i_{X\to Y} \le 0.2 \end{cases} \quad 1 \le i \le N - w + 1. \tag{2.10}$$

Similarly, $Type^i_{Y\to X}$ and $Intensity^i_{Y\to X}$ can be obtained by Eqs (2.9) and (2.10). Therefore, the state of the i_{th} fragment is defined. If $Type^i_{X\to Y} = N$, $Intensity^i_{X\to Y} = b$, $Type^i_{Y\to X} = P$, $Intensity^i_{Y\to X} = d$, the state of i_{th} fragment is $NbPd$. It means that the causality type from X to Y is negative, and the intensity is between 0.6 and 0.8; the causality type from Y to X is positive, and the intensity is between 0.2 and 0.4. According to this definition, the number of possible states is 225, and the combination rule is shown in Table 1.

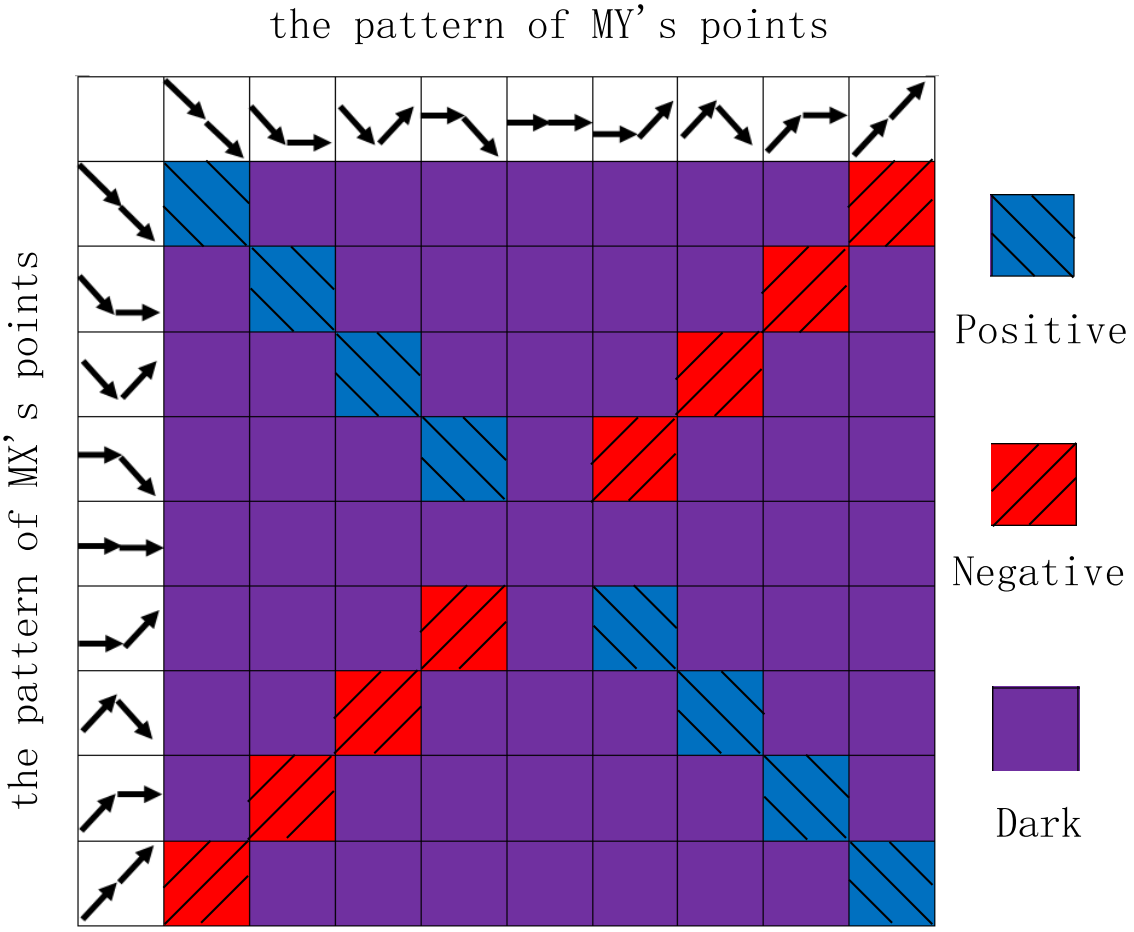

Figure 2. (color online) All the possible situations of PC patterns. The left blue striped box indicates that the real pattern $Pattern_{x(t)}$ and the estimated pattern $\hat{Pattern}_{x(t)}$ have the same pattern, i.e., the positive causality between $x(t)$ and $y(t)$. The right red striped box means that $x(t)$ and $y(t)$ have the opposite patterns, i.e., negative causality. The purple box represents the irregular pattern of $x(t)$ and $y(t)$, i.e., dark causality.

Table 1. The representation of state.

The first letter (the type of gold's influence on the dollar)	The second letter (the strength of gold's influence on the dollar)	The third letter (the type of dollar's influence on the gold)	The fourth letter (the strength of dollar's influence on the gold)
P	a, (0.8, 1] b, (0.6, 0.8] c, (0.4, 0.6] d, (0.2, 0.4] e, [0, 0.2]	P	a, (0.8, 1] b, (0.6, 0.8] c, (0.8, 0.6] d, (0.8, 0.4] e, [0, 0.2]
N	a, (0.8, 1] b, (0.6, 0.8] c, (0.4, 0.6] d, (0.2, 0.4] e, [0, 0.2]	N	a, (0.8, 1] b, (0.6, 0.8] c, (0.8, 0.6] d, (0.8, 0.4] e, [0, 0.2]
D	a, (0.8, 1] b, (0.6, 0.8] c, (0.4, 0.6] d, (0.2, 0.4] e, [0, 0.2]	D	a, (0.8, 1] b, (0.6, 0.8] c, (0.8, 0.6] d, (0.8, 0.4] e, [0, 0.2]

Step 5. Constructing the state-transition network.

We arranged states into a state chain according to the temporal order of appearance,

$$state^1 \rightarrow state^2 \rightarrow \cdots \rightarrow state^{N-w+1}, \tag{2.11}$$

in order to visualize the state chain, we mapped Eq (2.11) to a network by numbering each state, i.e., the first state *PaPa* as node 1, the second state *PaPb* as node 2, ..., the last state *DeDe* as node 225. Then, if two nodes appear adjacently, a directed edge is added between them. The network is called the directed and weighted state-transition network in which the direction is the order of the nodes appearing and the weight is the number of the edge between nodes.

2.3. Definitions of concepts

1) Degree: incoming degree or outgoing degree is defined as the number of incoming or outgoing links for a focused node. Note that the incoming (or outgoing) degree for a focused state (node) is equal to the number of occurrences of this state, except the state which appears in the first or last position in the state chain.

2) Hub node: nodes with extremely large degrees in the network.

3) Edge: if two states appear adjacently (i before j), a directed edge is added from i to j. The directed linkage has a clear physical meaning as the occurrence of the transition from i to j in the state chain [27, 28].

4) Edge weight: the edge weight indicates the strength of the relationship between the two connected nodes. Herein, the number of transfers between two nodes is defined as the weight of the edges between them. Note that this concept is very important, because we can obtained the transfer preferences between nodes based on this number. Moreover, according to the transition preferences from the focused state to other states, we can predict the subsequent state.

5) Shuffled data: the sequence is obtained by randomly disrupting the positions of the data in the original sequence.

6) Motif: if a node's degree for the original data is significantly larger than it in the shuffled data, the node is called a motif [39, 40].

7) Node's position sequence: the sequence of positions where the focused state (node) appears in the state chain.

8) Hurst index (H): a long-range correlation is common in actual data, which can be evaluated by estimating its Hurst index (scaling exponent). Different values of H indicate different evolution behaviors for the sequence. When $0 < H < 0.5$, the sequence shows anti-persistent evolution behavior, i.e., the state of the next moment is the opposite state of the previous one with large possibility; when $H = 0.5$, the characteristic of the sequence is a random walk, i.e., the two successive states of the sequence have no correlation; when $0.5 < H < 1$, a positive long-range correlation exists in the sequence, i.e., the next moment tends to maintain the same state as the previous one. The methods for estimating the Hurst index can be divided into the time-domain and frequency-domain methods. The time-domain methods include the variance-time method [41], the absolute values of the aggregated series method [41], the rescaled range analysis method (R/S) [42, 43] and the detrended fluctuation analysis method [44]; the frequency-domain methods include the periodic-diagram method [41], the whittle estimation method [45] and the wavelet analysis method [46].

9) Cluster: the cluster in the network is a sub-network for which the internal edges are denser and the external edges are sparse [47], i.e., nodes in the same cluster are more similar in specific attributes.

3. Results

3.1. Determination of an appropriate window size

In general, the window size w impacts results [48]. If w is too large, the rules of causality evolution between gold and the dollar will be obscured; while if w is too small, it will be more vulnerable to noise, and both the complexity and research cost will be higher. In addition, w also affects the number of states, that is, the larger w is, the less the number will be. In order to ensure the stability as well as diversity of the number of states, a balanced value for w is required.

The effect of the size w is examined from 100 to 1000 (the interval is 100) in that we obtain 10 state-transition networks. The numbers of nodes N_n and the numbers of edges N_e in state-transition networks are shown in Figure 3(a). The results show that both N_n and N_e for the shuffled sequence are more than that of the original sequence. In addition, both N_n and N_e for the original sequence decrease sharply with the increase of w when w is less than 600. When w is around 600, both N_n and N_e tends to be stable. On the contrary, both N_n and N_e for the shuffled sequence do not tend to be stable as that of the original sequence when w is around 600, i.e., the network structures of the shuffled sequence are not stable. Moreover, when w is 600 or 900, r_n or r_e are the smallest (i.e., the radio is the most deviated from 1), respectively (see Figure 3(b)). Herein, r_n and r_e represent the ratio of number of nodes of the original sequence to it of the shuffled sequence and the ratio of number of edges of the original sequence to it of the shuffled sequence, respectively. Accordingly, the difference between the original network and the shuffled network is the largest. Since the larger the w is, the more the information is lost and the higher the complexity is. Therefore, we assume that the reasonable value for w is 600 (i.e., a segment of around 840 days). Without special statement, w is selected as 600 through this article.

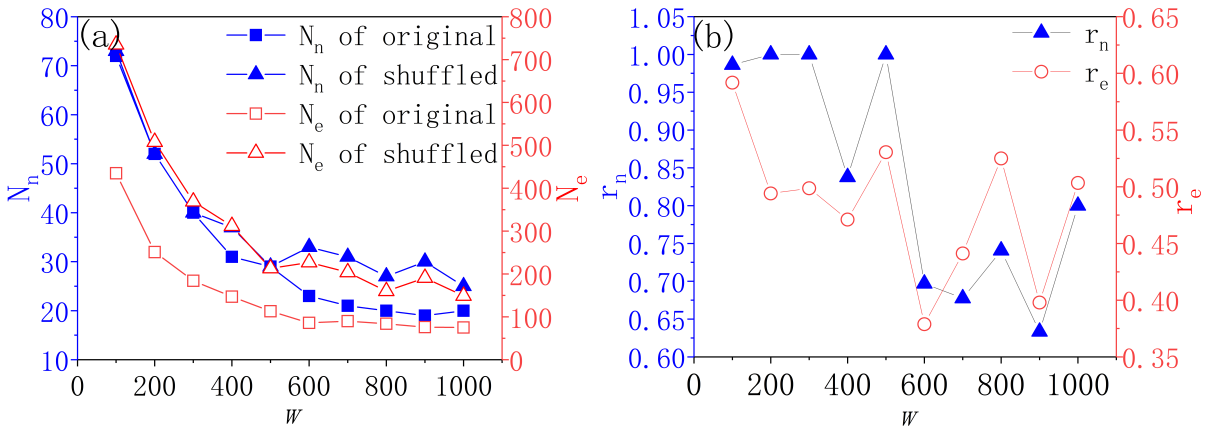

Figure 3. (color online) The effects of the window size w on the structures of the state-transition networks. (a) The effects of w on N_n as well as N_e in state-transition networks, where N_n and N_e represent the number of nodes and the number of edges, respectively. The solid rectangle and the solid triangle represent N_n for the original sequence and the shuffled sequence, respectively. The hollow rectangle and the hollow triangle represent N_e for the original sequence and the shuffled sequence, respectively. (b) The effects of w on r_n as well as r_e in the state-transition networks, where r_n and r_e represent the ratio of number of nodes of the original sequence to it of the shuffled sequences and the ratio of number of edges of the original sequence to it of the shuffled sequences, respectively.

3.2. Identification of important causality states

Figure 4 shows the state-transition networks for the original data (a) and the shuffled data (b), respectively. There are 23 nodes and 86 edges in (a) that are much smaller than 225 nodes and 225 × 225 = 50,625 edges for the all-to-all network. With regard to causality types, 10 nodes correspond to the states of negative causality from both directions (from gold to dollar and from dollar to gold), 4 nodes correspond to the states of dark causality from both directions, 9 nodes correspond to the state of negative causality from one direction and the state of dark causality from the other direction, and only one node 58 (i.e., State *PdDc*) corresponds to the state of positive causality from one direction and state of dark causality from the other direction. With respect to the causality intensity, only it of negative causality can be strong, i.e., larger than 0.6, whereas it of dark causality or positive causality is relatively low.

The state-transition network is heterogenous in (a). Most nodes have small degrees, whereas several hubs have large degrees. For example, both the incoming degree and outgoing degree are equal to 8 for Node 113 (i.e., State *NcNc*), and both the incoming degree and outgoing degree are 6 for Node 97 (i.e., State *NbNb*). Both Nodes 113 and 97 correspond to the states of negative causality from both directions. The edge weights are extremely heterogenous because the total weights of the two hubs' self-connecting edges are large, which ratio to the sum of the edge weights for the whole network is 68%. The self-connecting edges represent that when the focused state (node) appears, the state of the next moment remains the focused one. The state-transition network for the shuffled time series is shown in (b). The network is less heterogenous for the shuffled data. There are 33 nodes and 227 edges

in (b). Both the numbers of nodes and edges are relatively large and messy in this network, where only Node 193 (i.e., State *DcDc*) appears more frequently. State *DcDc* corresponds to the dark causality from both directions, which exists between two independently random sequences. In a word, the hubs of state-transition networks for the original data (a) and the shuffled data (b) correspond to the states of negative causality and dark causality from both directions, respectively.

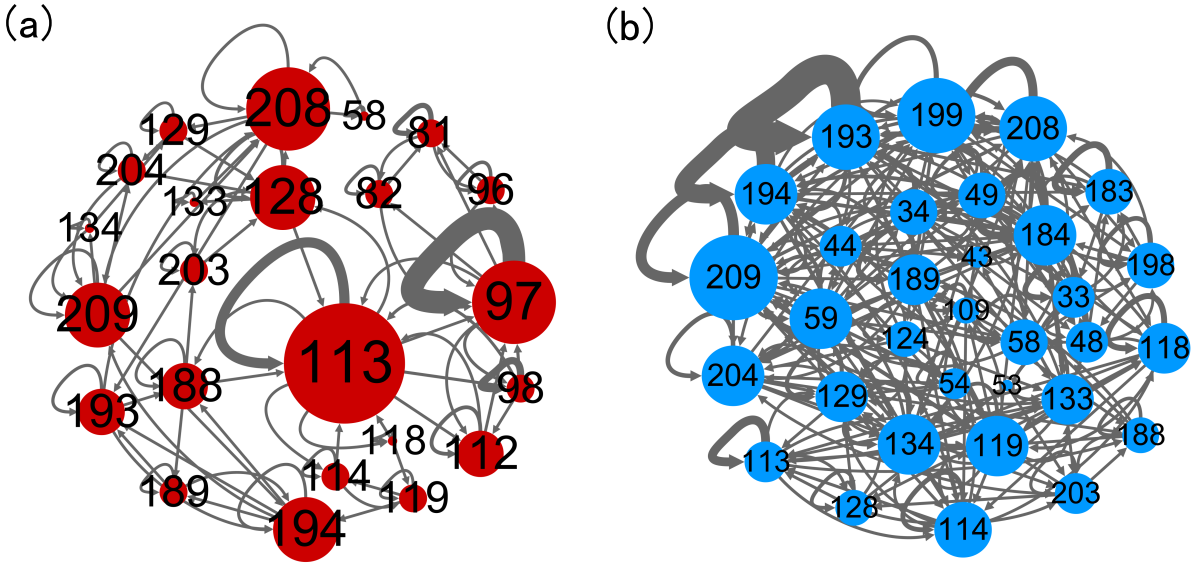

Figure 4. (color online) Diagrams for state-transition networks. (a) The state-transition network for the original bivariate time-series. (b) The state-transition network for the shuffled bivariate time-series. For visibility, the size of a node is proportional to its degree, and the thickness of an edge is proportional to its weight.

Figure 5 shows the comparison in the occurrence number of each state between the original data and the shuffled data. The numbers of occurrences for the two hubs (i.e., the incoming or outgoing degrees of Nodes 97 and 113) in the original data are apparently more than theirs in the shuffled data (a). Therefore, Nodes 113 and 97 are motifs. In addition, the number of occurrences for Node 193 in the shuffled data is visibly more than it in original data (a). Next, we examine whether the occurrence of the motifs are accidental or not. By the R/S method, we estimate the Hurst index for the time sequence composed of the positions where the nodes appear in turn in Figure 5(b)–(d). The Hurst indexes of Nodes 97 and 113 in the original data are larger than 0.5 ($H_{97,O} = 0.58$ and $H_{113,O} = 0.69$),respectively, and it of Node 193 in the shuffled data is close to 0.5 ($H_{193,S} = 0.51$). The results are entirely in line with intuitive expectations, i.e., the occurrences of Nodes 97 or 113 for the original data is long-range related, while the occurrence of Node 193 for the shuffled data is random.

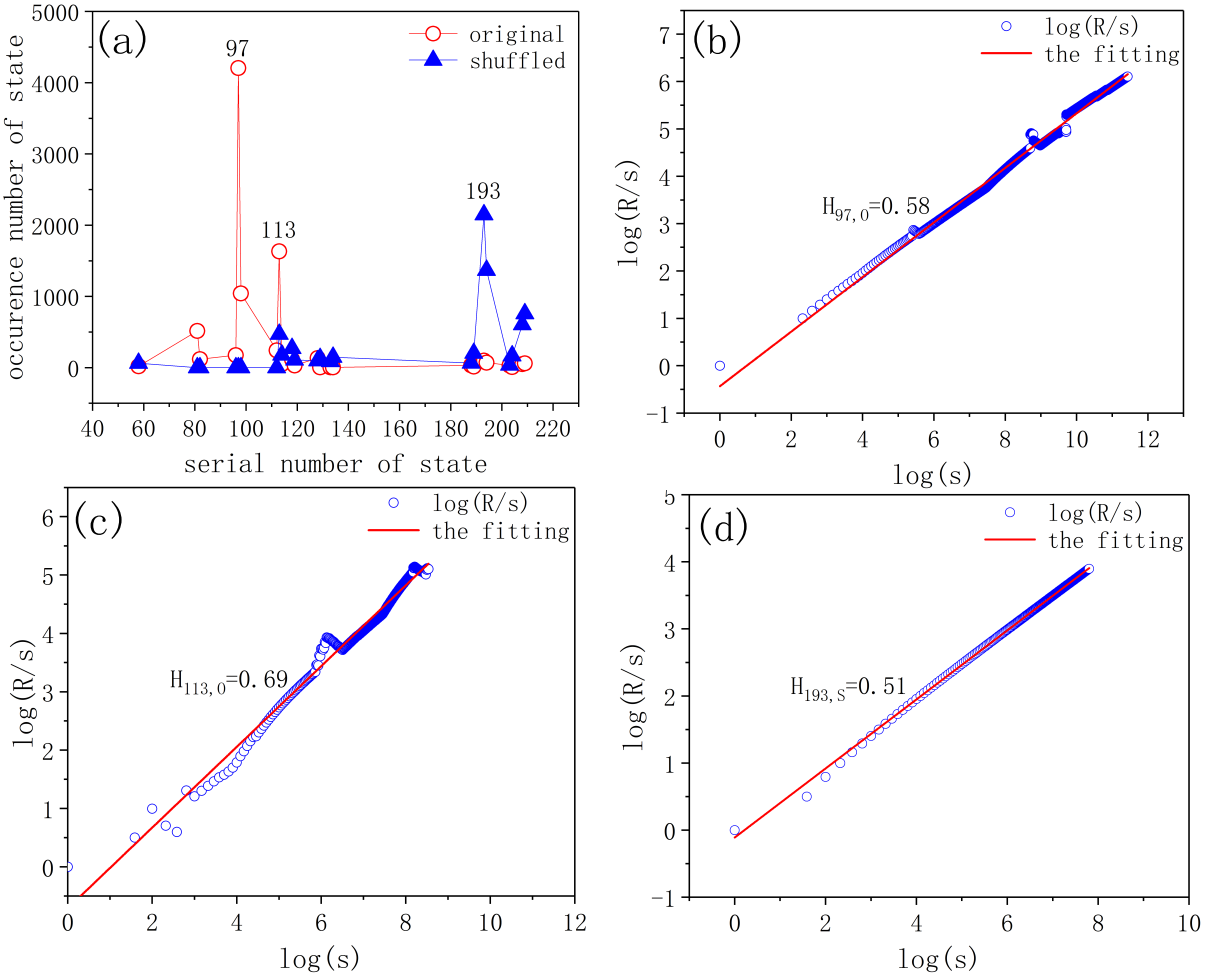

Figure 5. (color online) The comparison in the occurrences for each state between the original data and the shuffled data. The comparison in the number of occurrences for each state in (a). The Hurst indexes of the position sequence for Node 97 in (b) and Node 113 in (c) for the original data, and for Node 193 for the shuffled data (d).

3.3. Identification of the transitions between clusters

The importance of a node is reflected not only in the occurrence number but also in the probability of it transferring to other nodes. If the transition probability from one focused node to another is relatively large, the node of the next moment can be predicted when the focused node appears. Furthermore, if several nodes often transfer to each other, these nodes form a cluster.

In this article, a fast heuristic algorithm [49] is utilized to find the clusters. There are 4 clusters (see Figure 6), each of which mainly contains the same causality types as well as causality intensities. For simplicity, we let "weak" represents the causality intensity "d" or "e", "medium" represents the intensity "c", and "strong" represents the intensity "a" or "b". The largest cluster (Cluster *I*) is composed of 13 nodes that are mainly the states of weak dark causalities or the states of weak negative causalities. Although both the numbers of nodes and edges in Cluster *I* are the largest that are more than half of the whole network, the sum of its edge weights is meagre (see Figure 7(a)). In

the second largest cluster (Cluster *II*), four out of five nodes are the states of medium or strong negative causalities. Both the numbers of nodes and edges in Cluster *II* account for a small proportion, but the sum of its edge weights reaches 84% of the whole network (see Figure 7(a)). In the third largest cluster (Cluster *III*), all of the three nodes correspond to the states of strong negative causalities. In the smallest cluster (Cluster *IV*), both of the two nodes are the states of strong negative causalities. In order to show the transition within each cluster more clearly, (b)–(e) show the structures of the four clusters, respectively. It is visible that most edges within each cluster are bi-directional, in other words, they can mutually transfer to each other within the cluster.

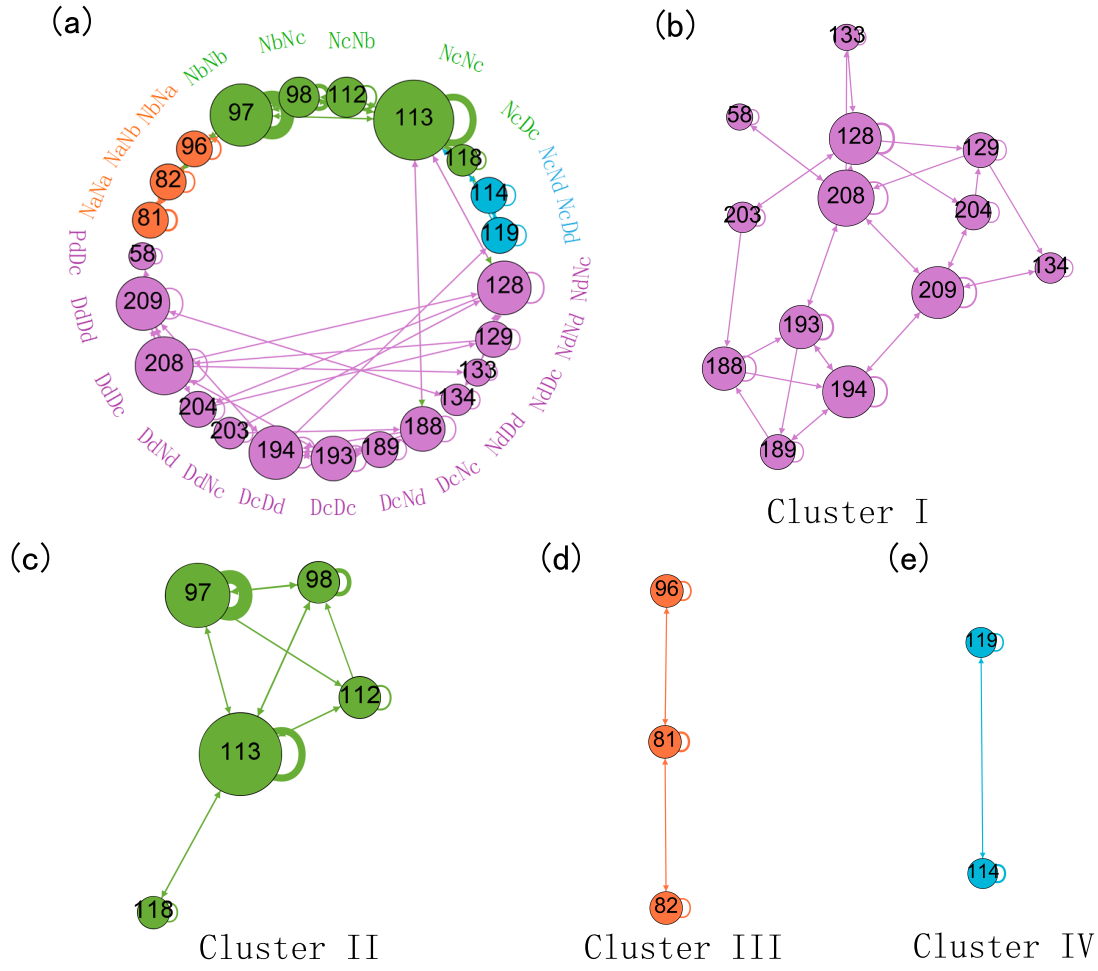

Figure 6. (color online) Clustering network diagram. (a) The original state-transition network is composed of four clusters. (b)–(e) the structures of the four clusters, respectively. Different colors represent different clusters. Note that Cluster *I* is mainly composed of states of weak dark causality, *II* states of strong or medium negative causality, *III* states of strong negative causality, and *IV* states of weak negative causality.

The connections across different clusters are different with the connections within each cluster. The edges across different clusters are much less than edges within the same cluster. The edges between clusters are very important, because they act as bridges in the transition across different clusters. Figure 7(b) shows the transition frequencies between clusters. Cluster *II* can transfer to the

other three clusters, and the other three can also transfer to Cluster *II*, whereas the other three can not transfer to each other. Therefore, Cluster *II* acts as a bridge in the transition among clusters. It means that even if there is a positive or dark causality (i.e., Cluster *I*, Cluster *III* or Cluster *IV*) between gold and the dollar, it is temporary and will soon transfer to Cluster *II*. Thus, we suggest that the relationship between gold and the dollar is the negative causality of being relatively stable for a long time. In a word, we can more accurately predict the causality between gold and the dollar next moment by these transition preferences of intra-cluster and inter-clusters.

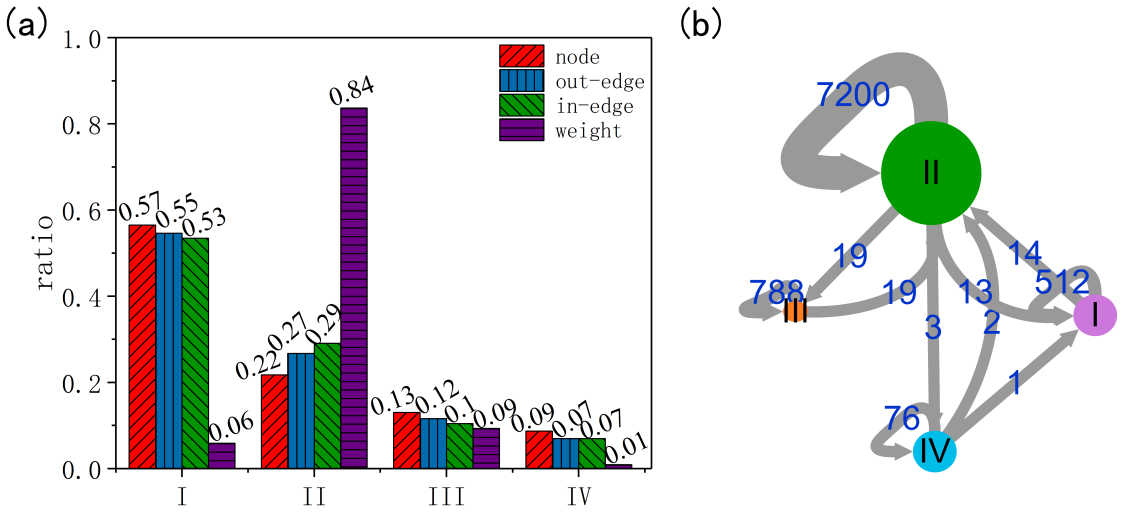

Figure 7. (color online) The characteristic diagram of the clusters. (a) The ratio of the statistics in each cluster to the whole network, including the number of nodes, the number of outgoing edges, the number of incoming edges and the sum of edge weights. (b) The transition diagram between the four clusters. Herein, the numbers marked in blue represent the times of transfers.

4. Conclusions and discussion

In this article, a method which combines the *PC* method [34, 35] and the state-transition network was developed to identify the characteristics of the causality evolution between gold and the dollar. Based on the *PC* method, we can identify not only the causality intensity but also the causality type in the segments of the bivariate time series, including the types of positive causality, negative causality and the dark causality. Then, both the causality type and the causality intensity were transformed into a particular state in each segment, i.e., a four-letter string. Finally, the state-transition network was built to detect the characteristics in the causality evolution between them, where the node is the causality state and the edge is the transition between states.

Two nodes (States *NbNb* and *NCNC*) were referred to motifs in the state-transition network. Surprisingly, both motifs corresponds to the strong or medium negative causality. The sum of the edge weights for these two motifs accounts for 68% of the total edge weights for the whole network, in other words, the number of appearances for these two states also accounts for 68% for the whole network. Thus, we suggest that the relationship between gold and the dollar is the negative causality of relatively stable for a long time, which corresponds to the previous research results [1, 15].

Several nodes form a cluster because they often transfer to each other. The transition preferences between causality states are compared between intra-cluster and inter-cluster. With regard to the intra-cluster, the transitions of nodes are not only frequent but also bidirectional. The nodes within the cluster can transfer to each other, but it is rare to transfer from one cluster to another. It is the other reason why the relationship between gold and the dollar is negative causality of being relatively stable for a long time. With respect to the inter-cluster, although the transitions across different clusters are much less than transitions within clusters, they play a key role in the connections (transitions) between different clusters. We found that Cluster *II* was especially essential. It can transfer to the other three clusters, and the other three can also transfer to Cluster *II*. However, the other three clusters can not transfer to each other. Therefore, Cluster *II* play a bridge role in the connections between clusters. It means that even if there is a positive or dark causality (i.e., Cluster *I*, Cluster *III* or Cluster *IV*) between gold and the dollar, it is temporary and will soon transfer to Cluster *II*. In a word, these transition preferences of intra-cluster and inter-clusters provide helpful information to evaluate the current causality between gold and the dollar, and to predict the causality of the next moment.

Different clusters are different in both the causality type and causality intensity of the nodes (states). Cluster *I* is mainly composed of states of weak dark causality, *II* states of strong or medium negative causality, *III* states of strong negative causality, and *IV* states of weak negative causality. It means that not only the causality type of nodes but also the causality intensity within each cluster are roughly the same. From this perspective, we can also explain the long-term stability of the negative causality between gold and the dollar.

As mentioned in [48], the window size w impacts results. By comparing the properties of the network constructed under different w, we found that the network structure tends to be stable when the w is around 600 (i.e., a segment of around 840 days). This discovery can provide a suitable time scale for future study.

The following suggestions may be of assistance to investors. Firstly, the number of appearances for two states accounts for 68% for the whole network. This indicates a negative correlation between gold and the dollar. That is, gold prices rise as the dollar depreciates, when investors are more likely to make more profits by investing in gold. Conversely, gold prices fall as the dollar appreciates, accordingly, it is a good time for investors to be short gold. Secondly, the existence of many self-connected edges in the network indicates that the relationship between them is difficult to change in short-term. Thus, it is risky for long-term investment, but for adventurous investors it can yield high returns in a short-term. Thirdly, investors should also consider the transition preferences of intra-cluster and inter-cluster when making investment decisions to reduce investment risk. For example, if the current relationship between gold and the dollar belongs to Cluster *II*, conservatives will likely believe the relationship will remain in Cluster *II* at the next moment (the self-connected edge weight is 7200), while adventurers will be more inclined to believe it will transfer to Cluster *III* (the transfer weight is 19). Finally, the length of 600 research window (i.e., a segment of around 840 days) is more conducive to the discovery of stable evolutionary rules that can assist investors in forming effective judgments.

Our research provides a new perspective to study the evolutional causality between two variables, i.e., gold and the dollar. In future, it is worth studying the evolutional causality between multiple variables, such as gold, the dollar, the price of crude oil, the financial crisis, and the political situation.

Acknowledgments

This work is supported by the National Natural Science Foundation of China under Grant No.11875042 and and the Natural Science Foundation of Shanghai under Grant No. 21ZR1443900.

Conflict of interest

The authors declare there is no conflicts of interest.

References

1. N. Apergis, Can gold prices forecast the Australian dollar movements? *Int. Rev. Econ. Finance*, **29** (2014), 75–82. http://doi.org/10.1016/j.iref.2013.04.004
2. T. D. Kaufmann, R. A. Winters, The price of gold: a simple model, *Resour. Policy* **15** (1989), 309–313. https://doi.org/10.1016/0301-4207(89)90004-4
3. B. Mo, H. Nie, Y. Jiang, Dynamic linkages among the gold market, US dollar and crude oil market, *Phys. A*, **491** (2017), 984–994. https://doi.org/10.1016/j.physa.2017.09.091
4. X. M. Ma, R. X. Yang, D. Zou, R. Liu, Measuring extreme risk of sustainable financial system using GJR-GARCH model trading data-based, *Int. J. Inf. Manage.*, **50** (2020), 526–537. https://doi.org/10.1016/j.ijinfomgt.2018.12.013
5. Z. H. Ding, K. Shi, B. Wang, Dollar's influence on crude oil and gold based on MF-DPCCA method, *Discrete Dyn. Nat. Soc.*, **2021** (2021), 5558967. https://doi.org/10.1155/2021/5558967
6. J. Chai, C. Y. Zhao, Y. Hu, Z. G. Zhang, Structural analysis and forecast of gold price returns, *J. Manage. Sci. Eng.*, **6** (2021), 135–145. https://doi.org/10.1016/j.jmse.2021.02.011
7. N. Diniz-Maganini, E. H. Dinizb, A. A. Rasheedc, Bitcoin's price efficiency and safe haven properties during the COVID-19 pandemic: a comparison, *Res. Int. Bus. Finance*, **58** (2021), 101472. https://doi.org/10.1016/j.ribaf.2021.101472
8. R. W. Jastram, The Golden Constant, *J. Econ.*, **100** (2010), 189–190. http://doi.org/10.1007/s00712-010-0124-5
9. B. M. Lucey, E. Tully, Seasonality, risk and return in daily comex gold and silver, *Appl. Financ. Econ.*, **16** (2006), 319–333. http://doi.org/10.1080/09603100500386586
10. M. Joy, Gold and the US dollar: hedge or haven? *Finance Res. Lett.*, **8** (2011), 120–131. http://doi.org/10.1016/j.frl.2011.01.001
11. C. S. Liu, M. S. Chang, X. M. Wu, C. M. Chui, Hedges or safe havens–revisit the role of gold and USD against stock: a multivariate extended skew-t copula approach, *Quant. Finance*, **16** (2016), 1763–1789. http://doi.org/10.1080/14697688.2016.1176238
12. K. Pukthuanthong, R. Roll, Gold and the Dollar (and the Euro, Pound, and Yen), *J. Banking Finance*, **35** (2011), 2070–2083. http://doi.org/10.1016/j.jbankfin.2011.01.014
13. J. C. Reboredo, Is gold a safe haven or a hedge for the US dollar? Implications for risk management, *J. Banking Finance*, **37** (2013), 2665–2676. http://doi.org/10.1016/j.jbankfin.2013.03.020

14. F. Capie, T. C. Mills, G. Wood, Gold as a hedge against the dollar, *J. Int. Financ. Mark., Inst. Money*, **15** (2005), 343–352. http://doi.org/10.1016/j.intfin.2004.07.002

15. M. Massimiliano, Z. Paolo, Gold and the U.S. dollar: tales from the turmoil, *Quant. Finance*, **13** (2013), 571–582. http://doi.org/10.2139/ssrn.1598745

16. F. L. Lin, Y. F. Chen, S. Y. Yang, Does the value of US dollar matter with the price of oil and gold? A dynamic analysis from time-frequency space, *Int. Rev. Econ. Finance*, **43** (2016), 59–71. https://doi.org/10.1016/j.iref.2015.10.031

17. H. An, X. Y. Gao, W. Fang, Y. Ding, W. Zhong, Research on patterns in the fluctuation of the co-movement between crude oil futures and spot prices: a complex network approach, *Appl. Energy*, **136** (2014), 1067–1075. https://doi.org/10.1016/j.apenergy.2014.07.081

18. A. L. Barabasi, R. Albert, Emergence of scaling in random networks, *Science*, **286** (1999), 509–512. https://doi.org/10.1126/science.286.5439.509

19. M. E. J. Newman, D. J. Watts, Renormalization group analysis of the small-world network model, *Phys. Lett.*, **263** (1999), 341–346. https://doi.org/10.1016/S0375-9601(99)00757-4

20. L. Lacasa, B. Luque, F. J. Ballesteros, J. Luque, J. C. Nuno, From time series to complex networks: the visibility graph, *Proc. Natl. Acad. Sci. U.S.A.*, **105** (2008), 4972–4975. http://doi.org/10.1073/pnas.0709247105

21. R. V. Donner, M. Small, J. F. Donges, N. Marwan, Y. Zou, R. Xiang, et al., Recurrence-based time series analysis by means of complex network methods, *Int. J. Bifurcation Chaos*, **21** (2011), 1019–1046. https://doi.org/10.1142/S0218127411029021

22. X. Y. Gao, W. Fang, F. An, Y. Wang, Detecting method for crude oil price fluctuation mechanism under different periodic time series, *Appl. Energy*, **192** (2017), 201–212. https://doi.org/10.1016/j.apenergy.2017.02.014

23. X. Han, Y. Zhao, M. Small, Identification of dynamical behavior of pseudoperiodic time series by network community structure, *IEEE Trans. Circuits Syst. II: Express Briefs*, **66** (2019), 1905–1909. https://doi.org/10.1109/TCSII.2019.2903936

24. Y. Zhao, T. Weng, S. Ye, Geometrical invariability of transformation between a time series and a complex network, *Phys. Rev. E*, **90** (2014), 012804. https://doi.org/10.1103/PhysRevE.90.012804

25. C. Zhou, L. Ding, Y. Zhou, H. Luo, Topological mapping and assessment of multiple settlement time series in deep excavation: a complex network perspective, *Adv. Eng. Inf.*, **36** (2018), 1–19. https://doi.org/10.1016/j.aei.2018.02.005

26. S. Mutua, C. G. Gu, H. j. Yang, Visibility graphlet approach to chaotic time series, *Chaos*, **26** (2016), 053107. http://doi.org/10.1063/1.4951681

27. Z. K. Gao, Q. Cai, Y. X. Yang, W. D. Dang, S. S. Zhang, Multiscale limited penetrable horizontal visibility graph for analyzing nonlinear timeseries, *Sci. Rep.*, **6** (2016), 035622. https://doi.org/10.1038/srep35622

28. Y. Y. Zhao, C. G. Gu, H. J. Yang, Visibility-graphlet approach to the output series of a Hodgkin-Huxley neuron, *Chaos*, **31** (2021), 043102. https://doi.org/10.1063/5.0018359

29. J. Zhang, D. C. Broadstock, The causality between energy consumption and economic growth for China in a time-varying framework, *Energy J.*, **37** (2016), 29–53. https://doi.org/10.5547/01956574.37.SI1.jzha
30. O. Nataf, L. De Moor, Debt rating downgrades of financial institutions: causality tests on single-issue CDS and iTraxx, *Quant. Finance*, **19** (2019), 1975–1993. https://doi.org/10.1080/14697688.2019.1619933
31. T. Wu, X. Y. Gao, S. F. An, S. Y. Liu, Diverse causality inference in foreign exchange markets, *Int. J. Bifurcation Chaos*, **31** (2021), 2150070. https://doi.org/10.1142/S021812742150070X
32. G. Sugihara, Detecting causality in complex ecosystems, *Science*, **338** (2012), 496–500. https://doi.org/10.1126/science.1227079
33. S. Y. Leng, H. F. Ma, J. Kurths, Y. C. Lai, W. Lin, K. Aihara, et al., Partial cross mapping eliminates indirect causal influences, *Nat. Commun.*, **11** (2020), 2632. http://doi.org/10.1038/s41467-020-16238-0
34. S. K. Stavroglou, A. A. Pantelous, H. E. Stanley, K. M. Zuev, Hidden interactions in financial markets, *Proc. Natl. Acad. Sci.*, **116** (2019), 10646–10651. http://doi.org/10.1073/pnas.1819449116
35. S. K. Stavroglou, A. A. Pantelous, H. E. Stanley, K. M. Zuev, Unveiling causal interactions in complex systems, *Proc. Natl. Acad. Sci.*, **117** (2020), 7599–7605. http://doi.org/10.1073/pnas.1918269117
36. G. Sugihara, R. M. May, Nonlinear forecasting as a way of distinguishing chaos from measurement error in time series, *Nature*, **344** (1990), 734–741. http://doi.org/10.1038/344734a0
37. F. Takens, Dynamical systems and turbulence, *Lect. Notes Math.*, Springer-Verlag, New York, **898** (1981), 366–381.
38. H. S. Kim, R. Eykholt, J. D. Salas, Nonlinear dynamics, delay times, and embedding windows, *Phys. D*, **127** (1999), 48–60. https://doi.org/10.1016/S0167-2789(98)00240-1
39. R. Milo, S. Shen-Orr, S. Itzkovitz, N. Kashtan, D. Chklovskii, U. Alon, Network motifs: simple building blocks of complex networks, *Science*, **298** (2002), 824–827. https://doi.org/10.1126/science.298.5594.824
40. A. Reka, A. Barabasi, Statistical mechanics of complex networks, *Rev. Mod. Phys.*, **74** (2002), 47–97. https://doi.org/10.1103/RevModPhys.74.47
41. M. S. Taqqu, V. Teverovsky, W. Willinger, Estimators for long-range dependence: an empirical study, *Fractals*, **3** (1995), 785–798. https://doi.org/10.1142/S0218348X95000692
42. H. E. Hurst, Long-term syorage capacity of reservoirs, *Trans. Am. Soc. Civ. Eng.*, **116** (1951), 770–799. https://doi.org/10.1061/TACEAT.0006518
43. E. E. Peters, *Fractal Market Analysis: Applying Chaos Theory to Investment and Economics*, Inc: John Wiley Sons, 1994. Available from: https://vdoc.pub/documents/fractal-market-analysis-applying-chaos-theory-to-investment-and-economics-2eb6d1gv7jsg.

44. A. Barulescu, C. Serban, C. Maftel, Evaluation of Hurst exponent for precipitation time series, in *Proceedings of the 14th WSEAS international conference on Computers: part of the 14th WSEAS CSCC multiconference*, (2010), 590–595. Available from: https://www.researchgate.net/publication/262253543.

45. P. M. Robinson, Gaussian semiparametric estimation of longrange dependence, *Ann. Stat.*, **23** (1995), 1630–1661. https://doi.org/10.1214/aos/1176324317

46. G. W. Wornell, A. V. Oppenheim, Estimation of fraetal signals from noisy measurements using wavelets, *IEEE Trans. Signal Process.*, **40** (1992), 611–623. https://doi.org/10.1109/78.120804

47. S. Fortunato, C. Castellano, Community structure in graphs, *Comput. Complexity*, Springer, New York, preprint, arXiv:0712.2716.

48. X. T. Sun, W. Fang, X. Y. Gao, S. F. An, S. Y. Liu, T. Wu, Time-varying causality inference of different nickel markets based on the convergent cross mapping method, *Resour. Policy*, **74** (2021), 102385. https://doi.org/10.1016/j.resourpol.2021.102385

49. V. D. Blondel, J. L. Guillaume, R. Lambiotte, E. Lefebvre, Fast unfolding of communities in large networks, *J. Stat. Mech.: Theory Exp.*, **10** (2008), P10008. https://doi.org/10.1088/1742-5468/2008/10/P10008

AIMS Press